Computational and Theoretical Polymer Science Vol. 7, No. 3/4, pp. 191–198, 1997

PII: S1089-3156(98)00005-1
0189-3156/98/$19.00 + 0.00

Molecular dynamics simulations of the thermal degradation of nano-confined polypropylene

Marc R. Nyden* and Jeffrey W. Gilman
Building and Fire Research Laboratory, National Institute of Standards and Technology, Gaithersburg, MD 20899, USA
(Received 8 October 1997; revised 12 December 1997)

Molecular dynamics simulations of the thermal degradation of polymer nanocomposites were performed in an attempt to explain the reduction in the flammability of these materials, as compared to the pure polymer, that has been observed in experimental measurements. The relative thermal stabilities of a series of polypropylene/graphite layered nanocomposites were assessed by comparing the rates of mass loss from model polymers as a function of the distance of separation between the graphite sheets. The effect of the interactions with the graphite was separated from the effect of nano-confinement of the polymer by comparing the results obtained from simulations where the nonbonding interactions between the polymer and the graphite were turned on to the corresponding values obtained when these interactions were turned off.

(Keywords: molecular dynamics simulations; thermal degradation; polymer nanocomposites)

INTRODUCTION

Recent work conducted in this laboratory has demonstrated that nanocomposites consisting of polymer and clay exhibit a significant reduction in flammability, as compared to the pure polymer, even at compositions that contain as little as 5% clay[1,2]. This increase in fire resistance is not achieved at the expense of compromising other physical properties. Indeed, in most cases, a dramatic improvement in the important thermal and mechanical properties is also observed[3,4]. Furthermore, the added costs associated with producing these composites from their components are expected to be almost negligible.

Experimental measurements have indicated that the rate of mass loss from polymer/clay nanocomposites exposed to fire-like heat fluxes is significantly reduced from the values observed for the pure polymer, while the enthalpies of combustion are almost identical[1,2]. This suggests that the source of the disparity in the flammability performances of these materials is due to differences in the condensed phase decomposition processes and not to a gas phase effect.

The purpose of this investigation is to identify the operant mechanisms for this increase in thermal stability and fire resistance. The strategy we have adopted to pursue this objective is to investigate the thermal decomposition of polymer nanocomposites using a computer model, hereafter referred to as MD_REACT, that was developed in this laboratory[5–8]. Although research in this area is just getting underway, preliminary results suggest that it is possible to make nanocomposites from a wide range of commodity polymers, thereby opening the way for the development of an entirely new generation of low cost, ultra fire resistant, high performance materials[1,2].

THEORY

The basis of MD_REACT is molecular dynamics. This technique involves solving

$$\frac{\partial H}{\partial p_i} = \frac{\mathrm{d}q_i}{\mathrm{d}t}, \quad \frac{\partial H}{\partial q_i} = -\frac{\mathrm{d}p_i}{\mathrm{d}t} \tag{1}$$

Hamilton's equations of motion for each of the 3N molecular degrees of freedom. In this equation, p_i and q_i are the Cartesian components of momentum and position, respectively. Molecular dynamics simulations are initiated by providing kinetic energy to the atoms from a random velocity distribution. The resulting distortions from the equilibrium geometry are opposed by a force

*To whom correspondence should be addressed. E-mail: mnyden@nist.gov

commensurate with the gradient of the Hamiltonian (H) in accord with equation (1).

The Hamiltonian used in the reactive dynamics simulations reported in this paper was derived from the Consistent valence force field (CVFF) developed by Molecular Simulations, Inc.* (MSI)[9]. The form of this Hamiltonian is summarised in equation (2).

$$H = \sum_{i}^{3N} \frac{p_i^2}{2m_i} + \sum_{ij}^{n\,\text{bonds}} V_b(r_{ij}) + \sum_{ijk}^{n\,\text{angles}} V_a(\theta_{ijk}) + \sum_{ijkl}^{n\,\text{torsions}} V_t(\phi_{ijkl}) + \sum_{ij}^{n\,\text{pairs}} V_{nb}(r_{ij}) \quad (2)$$

The first term on the right hand side of this equation represents the kinetic energy of the atoms and the next terms are the potential energies for bond stretching (V_b), bending (V_a) and a torsional potential (V_t) that restricts internal rotations of the covalent bonds. The last term represents the non-bond potential energy (V_{nb}) resulting from the electrostatic and Van der Waals interactions between all pairs of atoms that are not part of the same covalent bond angle (i.e. between atoms separated from each other by at least two atoms).

The unique capability of MD_REACT is that it allows for the formation of new bonds from free radical fragments generated when bonds in the polymer break and, thereby, accounts for the chemical reactions that play a major role in the thermal degradation process. The most important of these are bond scission, depolymerisation, hydrogen transfer, chain stripping, cyclisation, cross-linking and radical recombination reactions. The depolymerisation and intramolecular hydrogen transfer reactions, in particular, are modelled by introducing two new atom types (cf and ccf) into the CVFF force field to account for β-scission of carbon–carbon and carbon–hydrogen bonds. The ccf atom type corresponds to an aliphatic carbon (c) bonded to a free radical carbon (cf). Once a free radical is formed, the dissociation energies of the c–ccf and h–ccf bonds (beta to cf) are reduced by 317 kJ mol^{-1} (to 51 and 137 kJ mol^{-1}, respectively) which corresponds to the difference between a carbon–carbon single and double bond.

Radial switching functions are used to turn off the forces due to bending and twisting as the relevant bonds approach dissociation. The importance of including these terms in reactive force fields is elucidated in Ref. 10. The form of the switching functions used in the simulations performed in this investigation is given in equation (3)

$$S(ij) = \frac{1}{2}(1 - \tanh(a(r_{ij} - r_d))) \quad (3)$$

with $a = 40\,\text{nm}^{-1}$. The dissociation distances, r_d, are determined from an energy based criterion that depends on the nature of the atoms participating in the bond. The specific criterion adopted in MD_REACT is that atoms are converted to free radicals whenever the stretching energy in the bond between them approaches the average thermal energy, kT. A new set of bonds consisting of all possible covalent interactions between the available free radicals is formulated and those corresponding to the lowest energy subject to the constraints implicit in the valency of the atoms are retained. A more detailed description of the reactive force field used in the calculations reported in this paper can be found elsewhere [8].

Initially, the application of MD_REACT was limited to modelling simple vinyl polymers such as polyethylene. This constraint was overcome by interfacing our code with Discover 95, a commercial software package offered by MSI, that accesses both a much wider range of molecular structures and the extensive atomic force data that govern the thermal motion of polymers[11]. An integrated model, with the combined capabilities of both computer programs, was developed as part of a cooperative research and development agreement (CRADA) between BFRL/NIST and MSI.

PROCEDURE

The simulated thermal degradation experiments were performed on molecular models of polypropylene/graphite, rather than nylon/clay nanocomposites. In making this decision, we were motivated by the considerable body of experience and high level of confidence that we have acquired in using the CVFF force field to model hydrocarbon polymers and surfaces and we did not want to introduce any additional ambiguities into the interpretation of the computer simulations. The model of the polymer/graphite nanocomposite, consisting of four chains of isotactic polypropylene each containing 48 propylene monomers and a graphite sheet with about 600 carbon and 80 hydrogen (used to terminate the edges of the surface) atoms, is displayed in *Figure 1*.

A series of nanocomposite structures with the polymer intercalated between graphite layers

*Certain commercial equipment, instruments, materials, services or companies are identified in this paper in order to specify adequately the experimental procedure. This in no way implies endorsement or recommendation by NIST.

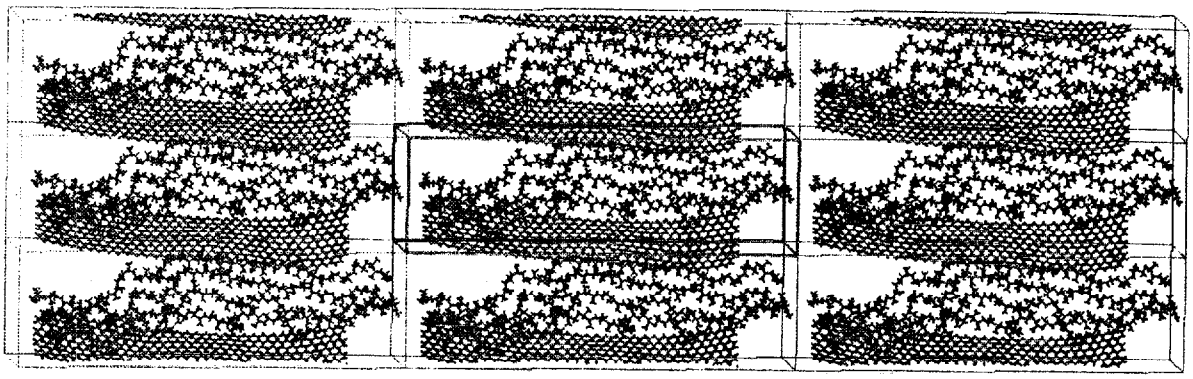

Figure 1 The model of the polymer/graphite nanocomposite, consisting of four chains of isotactic polypropylene each containing 48 propylene monomers and a graphite sheet with about 600 carbon and 80 hydrogen (used to terminate the edges of the surface) atoms

separated by a variable distance, b, was obtained by annealing the model polymer and graphite inside of a unit cell with the following dimensions: $a = 10.0$, $c = 3.0$ and $b = 2.5$, 2.8, 3.0, 3.2 and 5.0 nm. The same models of the polymer and graphite were used in all of the structures. That is, only the distance between the graphite sheets and, consequently, the density of the composite was allowed to change from one simulation to the next. The simulated annealing was performed by heating the polymer/graphite assembly to 500 K for 100 time steps and then relaxing it by performing 100 iterations of the Polak Ribiere conjugate gradient minimisation[9]. This sequence was performed 10 times. An energy optimised conformation was then obtained by minimising the full CVFF energy until the maximum derivative was less than $42\,J\,nm^{-1}\,mol^{-1}$. The entire process was repeated until the potential energy of the fully optimised structure was lower than any of the values attained during the course of the simulated annealing procedure.

The molecular dynamic simulations were performed using periodic boundary conditions in two stages. This strategy was adapted to resolve the disparity in the time scales corresponding to the initiation reactions, which have activation barriers on the order of $300\,kJ\,mol^{-1}$ or more, and the propagation/termination reactions which have activation barriers of $150\,kJ\,mol^{-1}$ or less. In the first stage of the simulation, a population of free radical polymer fragments was generated by integrating the equations of motion over a constant temperature path of 873 K for 50×10^{-15} s (50 time steps) using the full CVFF force field with cross terms coupling adjacent bonds, angles and torsions. The purpose of including cross terms, which are not represented in equation (2), was to facilitate an efficient transfer of thermal energy into the stretching modes that are responsible for bond dissociation. The bond stretching energies and forces were also scaled by a factor of 0.2 to further ensure that there was a sufficient population of free radical fragments to initiate the propagation and termination reactions (i.e. depolymerisation, hydrogen transfer, chain stripping, cyclization, crosslinking and radical recombination). This was deemed preferable to the alternative approach, which was to perform the simulations at unrealistically high temperatures (~2000 K) that might result in the occurrence of singular forces[10]. The bond scale factor was then set back to unity at the onset of the second stage where the propagation/termination reactions were simulated. This stage of the simulation was carried out at a constant temperature of 873 K for 5.0×10^{-12} s (5 000 time steps) using the reactive force field described in Ref. 8.

The mass loss was determined by tabulating the mass of the polymer fragments diffusing outside of the central unit cell as a function of time. These calculations were performed at intervals of 10^{-13} s providing a total of 51 instantaneous values for each simulation. The curves displayed in *Figures 4–8* were obtained by averaging data from three independent calculations corresponding to different realisations of the initial momentum distribution for the specified temperature of 873 K. The rate of mass loss was computed as the numerical derivative of this ensemble average. The time averaged rates, displayed in *Figure 9* as a function of the distance of separation between the graphite sheets, were obtained as the arithmetic means of the 51 instantaneous values corresponding to the ensemble averaged rate of mass loss for each of the nanocomposite structures. The uncertainties in these values, depicted as error bars in *Figure 9*, are the standard deviations of the time averaged rates from the three independent simulations.

The relative thermal stabilities of the polypropylene/graphite nanocomposites were assessed from the mass loss of the model polymer as a

function of the distance of separation between the graphite sheets. The effect of the interactions of the polymer with the graphite was separated from the effect of nano-confinement of the polymer by comparing the results obtained from simulations where the nonbonding interactions between the polymer and the graphite were turned on to the corresponding values obtained when these interactions were turned off. In either case, the positions and connectivities of the carbon and hydrogen atoms in the graphite were fixed throughout the simulations. This was done to make the simulations more computationally tractable. Benchmark studies, where these atoms were free to move, indicated that the deformations from the initial structure were minor and that the strategy of constraining the movement of the graphite was, therefore, a realistic approximation.

RESULTS AND DISCUSSION

In the absence of additives, the dominant mechanism in the thermal degradation of the model polypropylene is random scission of $CH–CH_3$ bonds followed by β-scission of the backbone to produce secondary free radical fragments and polymers with a vinyl end. The free radical polymer fragments then unzip releasing monomers until the degradation process terminates either by hydrogen transfer or radical recombination. This mechanism is summarised in *Figure 2*.

The rate of mass loss curve obtained from a typical simulation of the thermal degradation of polypropylene is displayed in *Figure 3*. The earliest peak coincides with the ejection of methyl groups from the polymer backbone. The following peaks correspond to depolymerisation and, later on, to

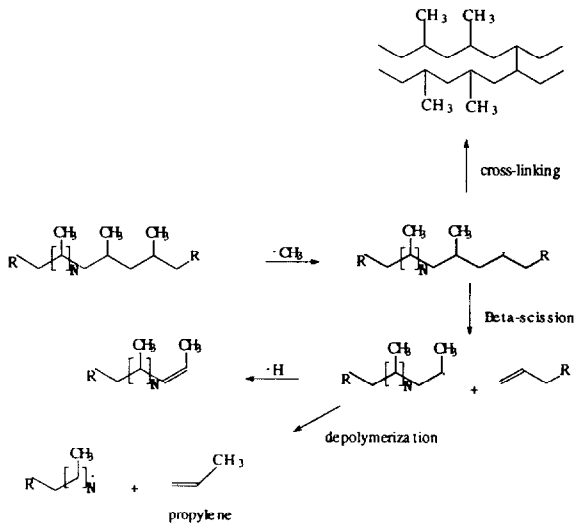

Figure 2 The predominant reactions in the thermal degradation of the model polymer

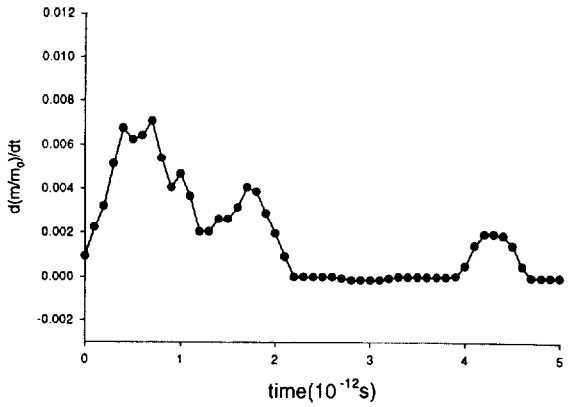

Figure 3 Rate of mass loss obtained from simulations of the thermal degradation of pure polypropylene

the diffusion of larger fragments (4, 5 and 6 carbons) that are produced as a result of multiple scission reactions. The rate at which the products of the thermal decomposition are transported through the polymer melt is clearly a strong function of molecular weight and fragments containing more than about 6 carbons do not usually have enough time to move out of the central unit cell during the 5×10^{-12} s extent of the simulations.

The mass loss curves from simulations of the thermal degradation of the nanocomposites (right) and the pure nano-confined polymers (left), obtained by turning-off the interactions with the graphite, are displayed in *Figure 4–8*. The effect of nano-confinement on the thermal stability of the model polymer can be assessed from the trends in the mass loss curves displayed on the left hand side of these figures. There is clearly an optimal polymer density that occurs when the distance of separation between the graphite layers is about 3.0 nm. At lower densities, the interactions with the polymer melt do not provide sufficient resistance to prevent the rapid diffusion of fragments to the gas phase, whereas the Van der Waals repulsions between the atoms destabilize the polymer when the density is too high. The latter effect is apparent in the dramatic increase in mass loss from the $b = 2.5$ nm nanocomposite. The consequences of the repulsive nature of the forces, that predominate when the polymer chains are crowded into the small volume bounded by the graphite sheets, is so pervasive that we could not even locate a stable conformation for a layered nanocomposite structure with b less than 2.5 nm using the simulated annealing procedure described in the previous section. In retrospect, this could have been anticipated because these nanocomposites are known to form delaminated, rather than layered, structures,when the mass fraction of polymer exceeds a critical value that corresponds to about 80% in the nylon-6/clay

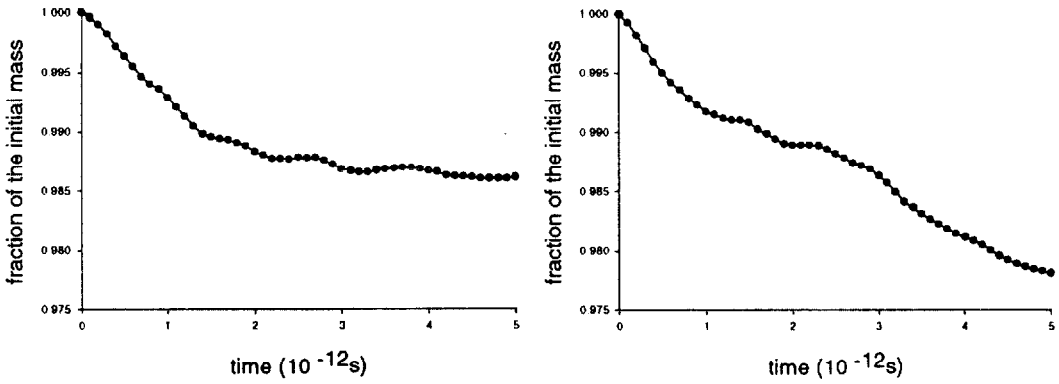

Figure 4 The mass loss curves from simulations of the thermal degradation of the $b = 2.5$ nm nanocomposite (right) and the pure nano-confined polymer (left) obtained by turning-off the interactions with the graphite

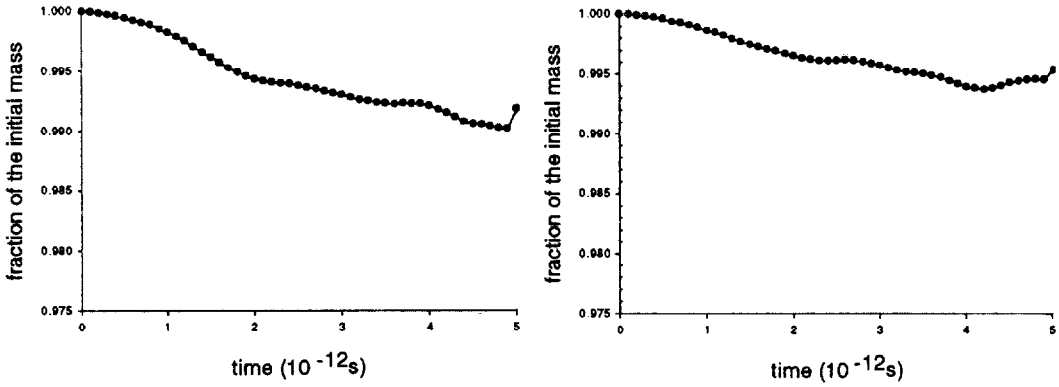

Figure 5 The mass loss curves from simulations of the thermal degradation of the $b = 2.8$ nm nanocomposite (right) and the pure nano-confined polymer (left) obtained by turning-off the interactions with the graphite

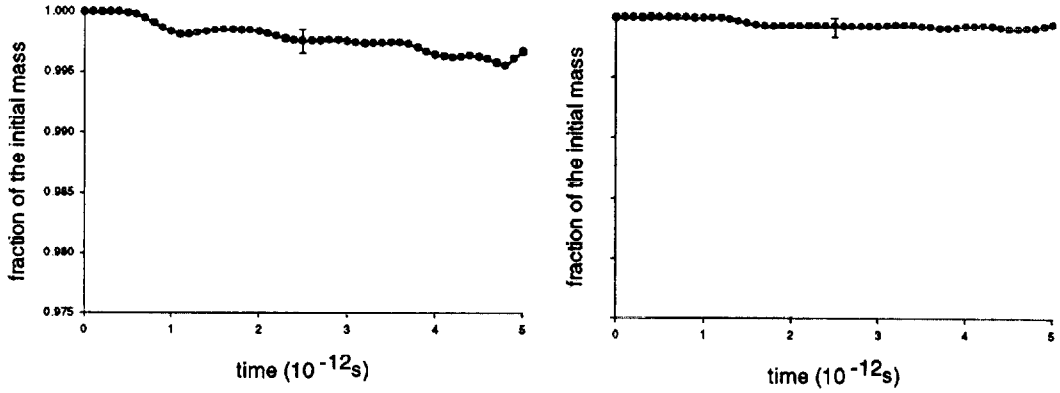

Figure 6 The mass loss curves from simulations of the thermal degradation of the $b = 3.0$ nm nanocomposite (right) and the pure nano-confined polymer (left) obtained by turning-off the interactions with the graphite

nanocomposites[3]. Presumably, the layered structure becomes unstable when the repulsive forces between the atoms that make-up the nano-confined polymer exceed the attractive forces between the layers. The clay then delaminates to form a hybrid structure where the layers are individually dispersed throughout the polymer matrix.

The interactions with the graphite impart an additional degree of stabilisation to the polymer at distances of separation between 2.8 nm and 3.2 nm that is evinced in the decrease in the slope of the mass loss curves when the interactions between the polymer and the graphite are turned on. The effect of these interactions appears to be destabilizing at $b = 2.5$ nm; however, the uncertainties in these particular values (*Figure 9*) are too high to draw a definitive conclusion.

The average rate of mass loss for both the pure nano-confined polymers and the nanocomposites are plotted as a function of the distance of separation

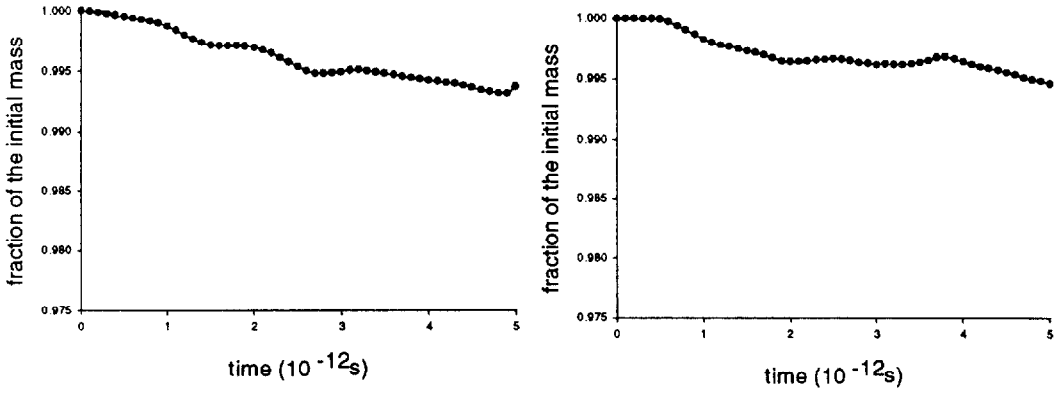

Figure 7 The mass loss curves from simulations of the thermal degradation of the $b = 3.2$ nm nanocomposite (right) and the pure nano-confined polymer (left) obtained by turning-off the interactions with the graphite

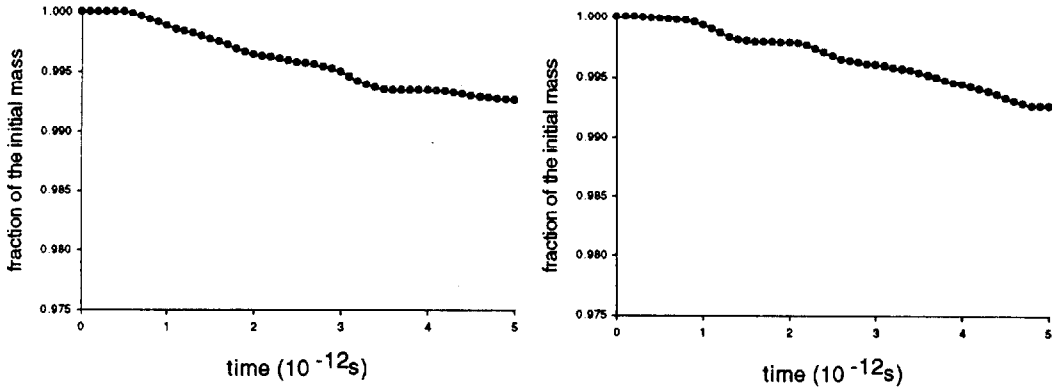

Figure 8 The mass loss curves from simulations of the thermal degradation of the $b = 5.0$ nm nanocomposite (right) and the pure nano-confined polymer (left) obtained by turning-off the interactions with the graphite

between the graphite layers in *Figure 9*. The stabilisation of the polymer is most pronounced in the $b = 3.0$ nm nanocomposite and approaches zero at $b = 5.0$ nm, when the graphite layers are too far apart for there to be a significant interaction between them. At these large distances of separation, the interactions are almost exclusively between the polymer and the graphite which should approximate what occurs in the delaminated nanocomposites where the graphite layers are individually dispersed in the polymer matrix. The reduction in the average rate of mass loss from the $b = 2.8$, 3.0 and 3.2 nm nanocomposites, with respect to the pure polymer, is consistent with the results obtained from radiative gasification experiments on intercalated nanocomposites [2]. The gasification apparatus used to make these measurements is specifically designed to emulate fire conditions by providing heat fluxes to the surface of the sample that are comparable to those experienced in a fire[12].

The observation that the thermal stability of the polymer increases when it is intercalated but is not affected by the presence of the clay when the layers delaminate is consistent with thermogravimetric data that indicate that intercalated nanocomposites are more thermally stable than delaminated nanocomposites[13,14]. Indeed, Gilman *et al.* noted that the derivative thermogravimetric (DTG) curves obtained from the delaminated nylon-6/clay nanocomposites are almost identical to the values corresponding to pure nylon-6, whereas the DTG curves of intercalated polystyrene/clay nanocomposites are shifted to dramatically higher temperatures than what is observed for pure

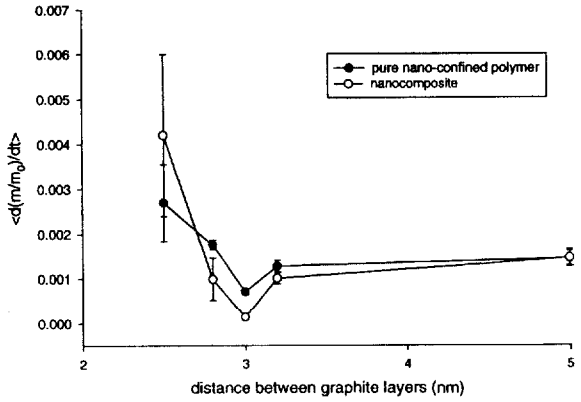

Figure 9 The average rate of mass loss for both the pure nano-confined polymers (filled circles) and the nanocomposites (open circles) are plotted as a function of the distance of separation between the graphite layers

polystyrene[2]. The fact that the delaminated nylon-6/clay nanocomposites exhibit a reduction in flammability comparable to what is observed for the intercalated nanocomposites, even though the DTG results indicate that polymers are not stabilised when present in delaminated nanocomposites, suggests the possibility that the clay layers reorganise after some of the polymer is gasified. That is, the nanocomposite undergoes a phase change from a delaminated to an intercalated structure as a result of the change in composition brought about by the thermal degradation of the polymer. Once the intercalated nanocomposite is formed, it is stabilized by the mechanism discussed in the preceding paragraphs. This hypothesis is supported by transmission electron microscopy (TEM) of the char that remained after burning samples of the delaminated nylon-6/clay nanocomposites under a thermal flux of $35\,kW\,m^{-2}$ on the cone calorimeter. The TEM images clearly reveal an organized layered structure that was not present prior to combustion[1,2].

The nature of the stabilisation effect is revealed in the computer animations of the trajectories corresponding to the nanocomposites and pure nano-confined polymers. In general, the polymers in the $b = 2.8$, 3.0 and 3.2 nm nanocomposites lost fewer fragments and retained their shape longer than the pure nano-confined polymers. The most obvious difference was that the fragments generated by the degradation of the model polymer in the nanocomposites had a pronounced tendency to collide with the graphite and bounce back into the central unit cell where they could undergo recombination reactions with other free radical polymer fragments, rather than escape from the melt as combustible fuel. This effect is evident in *Figure 10* which depicts the last frames from the animated trajectories of the pure polymer and the $b = 3.0$ nm nanocomposite. Notice that the fragments only escape from the sides of the nanocomposite (right) because of repulsive interactions with the graphite that bounds the polymer from above (not pictured) and below, whereas they leave the pure nano-confined polymer from all directions (left).

SUMMARY AND CONCLUSIONS

Molecular dynamics simulations of the thermal degradation of a series of polypropylene/graphite nanocomposites were performed as a function of the distance of separation between the graphite sheets. The mass loss curves obtained from these simulations indicate that there is a pronounced stabilisation of the polymer at $b = 3.0\,nm$ that results from both polymer–polymer and polymer–graphite interactions. The consequence of this stabilisation is a dramatic reduction in the average rate of mass loss that is consistent with the trends observed in radiative gasification experiments. The detailed nature of these interactions, including the dependence of the position and depth of the minimum, on the chemical nature of the polymer and solid, will be explored in future investigations.

ACKNOWLEDGEMENTS

We are honoured to be able to contribute a paper to this volume dedicated to the scientific accomplishments of Bruce Eichinger. One of us (M. R. N.) had the privilege of meeting Bruce while working on the code for MD_REACT as a visiting scientist at MSI in San Diego, and will always be grateful for the insightful advice that he offered on topics ranging from the best way to model polymers to how to buy a pair of roller blades. Thank you, Bruce, for that, and for all the important contributions that you have made, and continue to

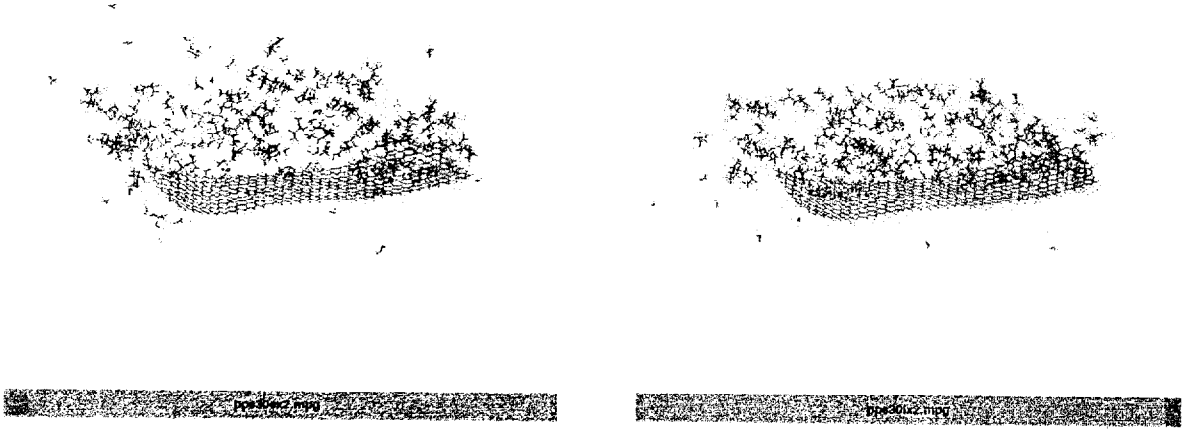

Figure 10 The last frames from the animated trajectories of the pure polymer (left) and the $b = 3.0$ nm nanocomposite (right)

make, to the field of polymer science. MD_REACT was developed as a result of a Cooperative Research and Development Agreement between NIST and Molecular Simulations Inc. (CRADA: CN-1241). Partial support for this work was provided by the Federal Aviation Administration under Interagency Agreement DTFA0003-92-Z-0018 monitored by Dr Richard E. Lyon. The authors would also like to acknowledge helpful discussions with Professor Emmanuel Giannelis and Dr Evangelos Manias of Cornell University.

REFERENCES

1. Gilman, J. W., Kashiwagi, T. and Lichtenhan, J. D., *SAMPE Journal*, 1997, **33**, 40.
2. Gilman, J. W., Kashiwagi, T., Lomakin, S., Lichtenhan, J. D., Jones, P., Giannelis, E. and Manias, E., Proceedings of the 6th European Meeting on Fire Retardancy of Polymeric Materials, Lille, France, September 1997.
3. Giannelis, E., *Adv. Mater* 1996, **8**, 19.
4. Kojima, Y., Usuki, A., Kawasumi, M., Okada, A., Fukushima, Y., Kurauchi, T. and Kamigaito, O., *J. Mater. Res.* 1993, **8**, 1185.
5. Nyden, M. R. and Noid, D. W., *Phys. Chem.* 1991, **95**, 940.
6. Nyden, M. R., Forney, G. P. and Brown, J. E., *Macromolecules*, 1992, **25**, 1658.
7. Nyden, M. R., Brown, J. E. and Lomakin, S. M., *Mat. Res. Soc. Symp. Proc.* 1992, **278**, 47.
8. Nyden, M. R., Coley, T. R. and Mumby, S., *Polym. Eng. Sci.* 1997, **37**(9), 1496.
9. *Discover User Guide, Part 3*, Molecular Simulations, San Diego, 1995.
10. Tuzun, R. E., Noid, D. W. and Sumpter, B. G., *Macromol. Theory Simul.* 1995, **4**, 909.
11. *Discover 95*, Biosym Solutions, Biosym Technologies, San Diego, Vol. 6, 1995.
12. Ritchie, S. J., Steckler, K. D., Hamins, A., Cleary, T. G., Yang, J. and Kashiwagi, T., The effect of sample size on the heat release rate of charring materials. Proceedings of the Fifth International Symposium on Fire Safety Science, 1997, 177.
13. Lee, J., Takekoshi, T. and Giannelis, E., *Mat. Res. Soc. Symp. Proc.*, 1997, **457**, 513.
14. Lee, J. and Giannelis, E., *Polymer Preprints*, 1997, **38**, 688.